Theory of nuclear excitation by inelastic muon scattering

Jie Zhou and Xu Wang*
Graduate School, China Academy of Engineering Physics, Beijing 100193, China

(Received 4 December 2025; revised 29 March 2026; accepted 1 May 2026; published 21 May 2026)

We develop a fully relativistic theoretical framework for calculating nuclear excitation cross sections induced by muon beams, covering a broad range of incoming energies from 1 to 1000 MeV. Focusing on experimentally accessible isotopes, ^{115}In and ^{90}Zr, we calculate excitation cross sections to various nuclear states. To enhance relevance for potential experiments, we also estimate the effective cross sections for excitation to long-lifetime isomeric states, suitable for postexcitation detection. Additionally, we compare the excitation cross sections for μ^-, μ^+, and electrons, and we assess the impact of muon penetration into the nucleus on these cross sections.

DOI: 10.1103/jzmn-zwdv

I. INTRODUCTION

Muons are fundamental particles with wide-ranging applications, including precision determination of nuclear properties [1–3], probing local magnetic environments in materials [4–6], imaging the internal structure of large or dense objects [7–9], and catalyzing nuclear reactions [10,11]. Consequently, numerous accelerator facilities worldwide routinely supply muon beams [12–17]. Recent demonstrations of intense-laser-based muon sources [18,19] further broaden access to muon beams.

Beyond static nuclear-structure studies [1–3], muons offer promising opportunities for active excitation and control of nuclei [20,21]. For example, nuclear excitation by muon capture has been shown to be more efficient than its electronic analog [20], and similar advantages arise in inelastic scattering for the case of ^{229}Th [21]. However, in contrast to the extensively explored electronic excitation channels [22–42], nuclear excitation by muons remains largely unexplored. To date, inelastic muon scattering has been studied only for ^{229}Th, and only at very low energies below 100 eV [21]. For general nuclei, however, excitation occurs at MeV-scale energies where relativistic effects become essential.

In this work, we present a general relativistic framework for nuclear excitation via inelastic muon scattering and apply it to two experimentally accessible nuclei, ^{115}In and ^{90}Zr. Both isotopes host long-lived isomeric states that allow for delayed, postexcitation detection. Within this framework, we calculate excitation cross sections to multiple nuclear levels and track the subsequent decay cascades feeding the isomeric state. Results for both μ^- and μ^+ projectiles are presented and compared with the corresponding electron-induced cases. We further evaluate the effect of muon penetration into the nuclear volume on nuclear excitation cross sections, using experimentally determined nuclear parameters and comparing predictions from different theoretical methods [43–45].

The paper is organized as follows. Section II introduces the theoretical framework for calculating muon-induced nuclear excitations. Section III presents excitation cross sections for ^{115}In and ^{90}Zr over a broad range of muon energies. Section IV summarizes the main findings.

II. THEORETICAL FRAMEWORK

A. Muon wave functions

The total electromagnetic interaction between a nucleus and a muon, expressed in atomic units ($m_e = e = \hbar = 1$), is given by the Hamiltonian [46]

$$H_I = \int \frac{\rho_\mu(\mathbf{r}_\mu)\rho_n(\mathbf{r}_n)}{|\mathbf{r}_\mu - \mathbf{r}_n|} d\mathbf{r}_\mu d\mathbf{r}_n - \frac{1}{c}\int [\mathbf{J}_\mu(\mathbf{r}) + \mathbf{J}_n(\mathbf{r})] \cdot \mathbf{A}(\mathbf{r}) d\mathbf{r}, \tag{1}$$

where $\mathbf{A}(\mathbf{r})$ is the vector potential of the radiation field, and $\rho_{\mu/n}$ and $\mathbf{J}_{\mu/n}$ denote the charge and current densities of the muon or the nucleus, respectively. The Coulomb gauge $\boldsymbol{\nabla} \cdot \mathbf{A} = 0$ is used. In muon scattering, the dominant interaction between the muon and the nuclear center of mass (with charge Z) is the Coulomb potential $e_\mu V(r) = e_\mu Z/r$, which governs the muon's scattering trajectory. Here $e_\mu = -1$ for μ^- and $+1$ for μ^+. The residual interaction between the muon and the internal nuclear degrees of freedom induces nuclear excitation, as discussed below.

The muon wave function $\phi(\mathbf{r})$ satisfies the Dirac equation

$$[-ic\boldsymbol{\alpha} \cdot \boldsymbol{\nabla} + \beta m_\mu c^2 + e_\mu V(r)]\phi(\mathbf{r}) = E\phi(\mathbf{r}), \tag{2}$$

where $\boldsymbol{\alpha}$ and β are the standard 4×4 Dirac matrices, c is the speed of light, $m_\mu = 206.77$ is the muon mass in atomic units, and E is the eigenenergy. For continuum states ($E > 0$), the solutions can be written in spherical coordinates as

$$|k\eta m\rangle = \frac{1}{r}\begin{pmatrix} P_{k\eta}(r)\Omega_{\eta m}(\theta,\varphi) \\ iQ_{k\eta}(r)\Omega_{-\eta m}(\theta,\varphi) \end{pmatrix}, \tag{3}$$

where k is the wave number, m is the magnetic quantum number, and $\eta = (l - j)(2j + 1)$ follows the usual definitions

*Contact author: xwang@gscaep.ac.cn

of the orbital angular momentum l and the total angular momentum j.

The radial functions satisfy the coupled equations

$$\frac{dP}{dr} = -\frac{\eta}{r}P + \frac{m_\mu c^2 + E - e_\mu V}{c}Q,$$
$$\frac{dQ}{dr} = \frac{m_\mu c^2 - E + e_\mu V}{c}P + \frac{\eta}{r}Q, \quad (4)$$

while the angular component is given by

$$\Omega_{\eta m}(\theta,\phi) = \sum_{s=\pm 1/2}\left\langle \frac{1}{2}, l, s, m-s | jm\right\rangle Y_{l,m-s}(\theta,\phi)\chi_s, \quad (5)$$

with χ_s being the Pauli spinors and $\langle\cdots|\cdots\rangle$ the Clebsch-Gordan coefficients. The continuum eigenstates $|k\eta m\rangle$ are normalized on the wave-number scale in our calculations.

The initial and final muon states before and after scattering are described by distorted waves (DW), $|\phi_i\rangle = |\mathbf{k}_i s_i\rangle^{(+)}$ and $|\phi_f\rangle = |\mathbf{k}_f s_f\rangle^{(-)}$. Using partial-wave expansion, these states can be written as

$$|\mathbf{k}s\rangle^{(\pm)} = \frac{4\pi}{k}\sqrt{\frac{E+m_\mu c^2}{2E}}\sum_{\eta m}\exp(\pm i d_{E\eta})$$
$$\times[\Omega^\dagger_{\eta m}(\theta_k,\varphi_k)\chi_s]|k\eta m\rangle, \quad (6)$$

where $d_{E\eta}$ is the scattering phase shift [47]. For the numerical solution of the Dirac equation, we employ the publicly available RADIAL code [48]. Although originally designed for electron wave functions, it can be used for both positive and negative muons by simply replacing the electron mass and charge in Eq. (4).

B. Nuclear wave functions

In this work, we do not compute the many-body nuclear wave functions (denoted $|\psi\rangle$) for several reasons. (i) As shown below, all necessary nuclear-structure information enters our formulation through the reduced transition probabilities $B(\mathcal{T}\lambda)$. (ii) Accurate many-body calculations for medium-to-heavy nuclei—such as the ^{115}In and ^{90}Zr isotopes considered here [49–51]—remain computationally demanding and lie beyond the scope of this study. (iii) A practical and widely adopted approach in Coulomb-excitation theory is to use experimentally measured $B(\mathcal{T}\lambda)$ values whenever available [28,31,46,52]. We follow this standard strategy here.

C. Eigenmodes of the electromagnetic field

There are two classes of electromagnetic-wave eigenmodes in a spherical cavity of radius R: the electric (E-type) and magnetic (M-type) modes. Each mode is labeled by the angular momentum quantum number λ, the magnetic quantum number ν, and the wave number κ. Their vector potentials are

$$\mathbf{A}(E\lambda,\nu,\kappa) = \sqrt{\frac{8\pi c^2}{\lambda(\lambda+1)R}}\nabla\times\mathbf{L}[j_\lambda(\kappa r)Y_{\lambda\nu}(\theta,\phi)] \quad (7)$$

and

$$\mathbf{A}(M\lambda,\nu,\kappa) = i\sqrt{\frac{8\pi c^2K^2}{\lambda(\lambda+1)R}}\mathbf{L}[j_\lambda(\kappa r)Y_{\lambda\nu}(\theta,\phi)], \quad (8)$$

where $\mathbf{L}$ is the angular momentum operator and j_λ is the λ-order spherical Bessel function.

The quantized field $\mathbf{A}$ can be expanded as

$$\mathbf{A} = \sum_{\lambda\nu\kappa}[a(E\lambda,\nu,\kappa)\mathbf{A}(E\lambda,\nu,\kappa) + a(M\lambda,\nu,\kappa)\mathbf{A}(M\lambda,\nu,\kappa) + \text{H.c.}], \quad (9)$$

where the annihilation operation a satisfies

$$ME\langle n'|a|n\rangle = \sqrt{\frac{n}{2\kappa c}}\delta_{n,n'+1} \quad (10)$$

in the Fock representation.

D. Nuclear excitation

As mentioned above, the interaction potential responsible for nuclear excitation is $H_{\mu n} = H_I - e_\mu V$. The initial and final states of the system are written as $|i\rangle = |\phi_i\rangle\otimes|\psi_i\rangle\otimes|0\rangle$ and $|f\rangle = |\phi_f\rangle\otimes|\psi_f\rangle\otimes|0\rangle$, respectively. We use $|\phi\rangle$ to denote the muon state, $|\psi\rangle$ the nuclear state, and $|0\rangle$ the vacuum state of the radiation field. The transition matrix element is given to the second order as

$$T_{fi} \approx \langle f|H_{\mu n}|i\rangle + \sum_g \frac{\langle f|H_{\mu n}|g\rangle\langle g|H_{\mu n}|i\rangle}{E_i - E_g}, \quad (11)$$

where $|g\rangle = |\phi_g\rangle\otimes|\psi_g\rangle\otimes|1\rangle$ are one-photon intermediate states, and E_i and E_g are the energies of the corresponding states.

In general, the muon and nuclear degrees of freedom are entangled in T_{fi}, making it difficult to evaluate integrals of the form

$$F = \int \frac{\phi_i(\mathbf{r}_\mu)\phi_f(\mathbf{r}_\mu)\psi_i(\mathbf{r}_n)\psi_f(\mathbf{r}_n)}{|\mathbf{r}_n - \mathbf{r}_\mu|}d\mathbf{r}_n d\mathbf{r}_\mu \quad (12)$$

without an explicit representation of the nuclear wave function ψ. However, in many situations—particularly when the muon energy is low—the spatial overlap between the muon and the nucleus is negligible. That is, for essentially any position $\mathbf{r}$, either $\phi(\mathbf{r}) \approx 0$ or $\psi(\mathbf{r}) \approx 0$. Under this condition, the muon and nuclear coordinates can be effectively disentangled in the denominator, and the T-matrix element simplifies to the form given below:

$$T_{fi} \approx 4\pi\sum_{\lambda\nu}[\langle\phi_f|\mathcal{N}(E\lambda,\nu,q)|\phi_i\rangle\langle\psi_f|\mathcal{M}(E\lambda,-\nu,q)|\psi_i\rangle - \langle\phi_f|\mathcal{N}(M\lambda,\nu,q)|\phi_i\rangle\langle\psi_f|\mathcal{M}(M\lambda,-\nu,q)|\psi_i\rangle] \times\frac{(-1)^\nu}{2\lambda+1}. \quad (13)$$

Here, multipole operators

$$\mathcal{N}(E\lambda,\nu,q)=\frac{iq^{\lambda}}{c\lambda(2\lambda-1)!!}\times\int\mathbf{J}_{\mu}(\mathbf{r})\cdot\nabla\times\mathbf{L}\big[h_{\lambda}^{(1)}(qr)Y_{\lambda\nu}(\theta,\varphi)\big]\mathrm{d}\mathbf{r},$$

$$\mathcal{M}(E\lambda,\nu,q)=\frac{(2\lambda+1)!!}{cq^{\lambda+1}(\lambda+1)}\times\int\mathbf{J}_{n}(\mathbf{r})\cdot\nabla\times\mathbf{L}[j_{\lambda}(qr)Y_{\lambda\nu}(\theta,\varphi)]\mathrm{d}\mathbf{r},$$

$$\mathcal{N}(M\lambda,\nu,q)=\frac{q^{\lambda}}{c\lambda(2\lambda-1)!!}\times\int\mathbf{J}_{\mu}(\mathbf{r})\cdot\mathbf{L}\big[h_{\lambda}^{(1)}(qr)Y_{\lambda\nu}(\theta,\varphi)\big]\mathrm{d}\mathbf{r},$$

$$\mathcal{M}(M\lambda,\nu,q)=\frac{-i(2\lambda+1)!!}{cq^{\lambda+1}(\lambda+1)}\times\int\mathbf{J}_{n}(\mathbf{r})\cdot\mathbf{L}[j_{\lambda}(qr)Y_{\lambda\nu}(\theta,\varphi)]\mathrm{d}\mathbf{r}\tag{14}$$

are introduced, where $h_{\lambda}^{(1)}$ is the λ-order spherical Hankel function of the first kind and $q=(E_i-E_f)/c$ is the wave number of the virtual photon. In addition, since $qr\ll 1$ holds inside the nucleus, the asymptotic form [53]

$$j_{\lambda}(qr)\approx\frac{(qr)^{\lambda}}{(2\lambda+1)!!}\tag{15}$$

is available to match the reduced nuclear $\mathcal{T}\lambda$-transition probability ($\mathcal{T}=E,M$) as

$$B(\mathcal{T}\lambda,i\to f)\approx\sum_{\nu M_f}|\langle N_fI_fM_f|\mathcal{M}(\mathcal{T}\lambda,\nu,q)|N_iI_iM_i\rangle|^2.\tag{16}$$

Assuming the incoming direction $\mathbf{k}_i$ is along the z axis, the differential cross section for nuclear excitation is

$$\frac{d\sigma_{if}}{d\Omega}=\frac{E_iE_fk_f}{8\pi^2c^4k_i}\sum_{s_is_f}|T_{fi}|^2,\tag{17}$$

after averaging over the muon spin s_i and summing over s_f [34]. The total cross section is

$$\sigma_{if}=8\pi^2\frac{(E_f+m_{\mu}c^2)(E_i+m_{\mu}c^2)}{k_fk_i^3}\sum_{\mathcal{T}\lambda}\frac{q^{2\lambda+2}}{[(2\lambda+1)!!]^2}\cdot B(\mathcal{T}\lambda,i\to f)C_{if}^{\mathcal{T}\lambda}.\tag{18}$$

For $E\lambda$ terms,

$$C_{if}^{E\lambda}=\sum_{\eta_i\eta_f}(2j_i+1)(2j_f+1)(2l_i+1)(2l_f+1)\times\begin{pmatrix}l_i&\lambda&l_f\\0&0&0\end{pmatrix}^2\begin{Bmatrix}l_i&\lambda&l_f\\j_f&1/2&j_i\end{Bmatrix}^2\left|\mathcal{R}_{if}^{E\lambda}\right|^2\tag{19}$$

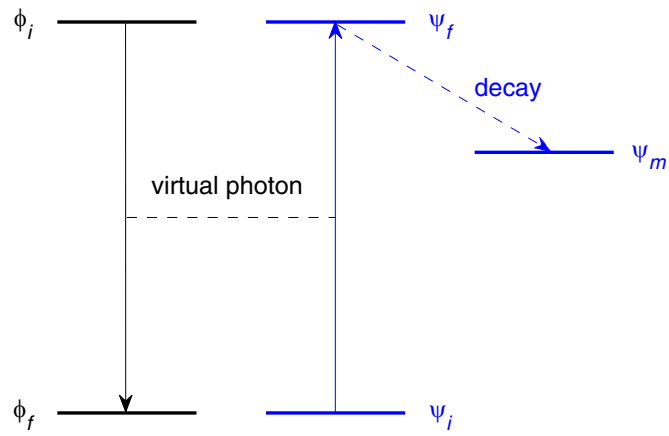

FIG. 1. Illustration of generating a nuclear isomeric state ψ_m. The nucleus is excited from ψ_i to ψ_f by exchanging a virtual photon with the muon, the state of which changes from ϕ_i to ϕ_f. Then the nucleus rapidly decays into the isomeric state ψ_m directly or through intermediate states.

and

$$\mathcal{R}_{if}^{E\lambda}=\int\left\{h_{\lambda}^{(1)}(qr)[P_i(r)P_f(r)+Q_i(r)Q_f(r)]+\frac{h_{\lambda-1}^{(1)}(qr)}{\lambda}[(\eta_i-\eta_f+\lambda)P_f(r)Q_i(r)+(\eta_i-\eta_f-\lambda)P_i(r)Q_f(r)]\right\}dr.\tag{20}$$

For $M\lambda$ terms, the parameter $l_i'=2j_i-l_i$ is used:

$$C_{if}^{M\lambda}=\sum_{\eta_i\eta_f}(2j_i+1)(2j_f+1)(2l_i'+1)(2l_f+1)\times\begin{pmatrix}l_i'&\lambda&l_f\\0&0&0\end{pmatrix}^2\begin{Bmatrix}l_i'&\lambda&l_f\\j_f&1/2&j_i\end{Bmatrix}^2\left|\mathcal{R}_{if}^{M\lambda}\right|^2\tag{21}$$

and

$$\mathcal{R}_{if}^{M\lambda}=\frac{\eta_i+\eta_f}{\lambda}\int h_{\lambda}^{(1)}(qr)[P_i(r)Q_f(r)+Q_i(r)P_f(r)]dr.\tag{22}$$

E. Production of isomers

Direct excitation from the initial nuclear state $|\psi_i\rangle$ to the isomeric state $|\psi_m\rangle$ is typically very inefficient, owing to the large angular-momentum difference between them—precisely the reason for the isomer's long lifetime. Instead, the isomeric state is populated through indirect pathways, as illustrated in Fig. 1: the nucleus is first excited to a higher-lying state $|\psi_f\rangle$, which then decays rapidly into the isomer, either directly or through one or more intermediate levels.

The effective isomeric excitation cross section from $|\psi_i\rangle$ to $|\psi_m\rangle$ is therefore

$$\sigma_{im}=\sum\sigma_{if}b_{fg}b_{gh}\ldots b_{lm},\tag{23}$$

TABLE I. Reduced nuclear transition probability $B(\mathcal{T}\lambda, i \to f)$ of ^{115}In and ^{90}Zr in Weisskopf units from the ground state $|\psi_i\rangle$ to excited states $|\psi_f\rangle$. All nuclear energy levels $\mathcal{E}$ are given in keV.

^{115}In			^{90}Zr		
$\mathcal{E}_f$	$\mathcal{T}\lambda$	$B(\mathcal{T}\lambda, i \to f)$	$\mathcal{E}_f$	$\mathcal{T}\lambda$	$B(\mathcal{T}\lambda, i \to f)$
934	$M1$	3.76×10^{-4}	2748	$E3$	56
941	$E2$	0.792	4229	$E2$	0.47
1078	$E2$	6.66	4681	$E2$	0.49
1449	$E2$	4.5	4701	$E2$	0.084
1449	$M1$	1.9×10^{-4}	4824	$E2$	0.155
1464	$E2$	1.36	5437	$E2$	0.185
1464	$M1$	0.04	5591	$E2$	0.405
1486	$E2$	2			
1486	$M1$	6.4×10^{-3}			

where the sum runs over all decay chains of the form

$$|\psi_f\rangle \to |\psi_g\rangle \to |\psi_h\rangle \to \cdots \to |\psi_l\rangle \to |\psi_m\rangle. \quad (24)$$

Here, each b denotes a branching ratio; for example, b_{fg} is the fraction of decays from $|\psi_f\rangle$ that proceeds directly to $|\psi_g\rangle$.

III. RESULTS AND DISCUSSIONS

A. Nuclear excitation cross sections

We illustrate our approach using ^{115}In and ^{90}Zr, both of which are stable nuclei and experimentally accessible. ^{115}In has an isomeric state at 336 keV with a half-life of 4 h, and ^{90}Zr has an isomeric state at 2319 keV with a half-life of 0.8 s. All other excited states included in our calculations have half-lives shorter than 0.1 ns. The reduced nuclear transition probability B (Table I) and the branching ratios b (Table II) are taken from the Nuclear Structure and Decay Databases [54].

The cross sections for direct nuclear excitation to various excited states are shown in Fig. 2 for (a) ^{115}In and (b) ^{90}Zr. For ^{115}In, the cross sections are quite similar for most final states, ranging from 10^{-28} to 10^{-27} cm^2 over a broad muon energy range from 2 to 1000 MeV. An exception is the 934-keV excited state, whose cross section is 4 to 5 orders of magnitude smaller. This is due to the fact that the transition to the 934-keV state is predominantly of the $M1$ type, which is less efficient than $E2$ transitions in muon excitation [21]. For other excited states, $E2$ transitions are the dominant channels.

For ^{90}Zr, the cross sections are generally on the order of 10^{-30} to 10^{-29} cm^2, with the exception of the more efficient 2748-keV state. The transition to this state is of the $E3$ type, which is more efficient than the $E2$ transitions to other states, particularly at higher muon energies.

The efficiency of nuclear transition types is influenced by several factors. The reduced transition probability $B(\mathcal{T}\lambda)$ is clearly a key factor, as it is proportional to the cross sections and largely determines the distinct behavior of the

TABLE II. Branching ratios b_{fg} of ^{115}In and ^{90}Zr from state $|\psi_f\rangle$ to state $|\psi_g\rangle$.

^{115}In			^{90}Zr		
$\mathcal{E}_f$	$\mathcal{E}_g$	b_{fg}	$\mathcal{E}_f$	$\mathcal{E}_g$	b_{fg}
597	336	1.00	2739	2319	1.00
829	336	0.92	2748	2319	5.0×10^{-3}
829	597	8.4×10^{-2}	3077	2319	2.4×10^{-2}
934	829	2.2×10^{-3}	3077	2739	8.2×10^{-3}
941	597	0.10	3077	2748	6.1×10^{-2}
1078	597	0.16	4229	2748	0.34
1078	941	1.0×10^{-2}	4681	2748	0.50
1449	934	5.0×10^{-3}	4701	2748	0.40
1449	941	1.3×10^{-2}	4824	3077	6.4×10^{-2}
1449	1078	4.0×10^{-4}	5437	2748	0.61
1464	1078	5.8×10^{-2}	5591	2748	0.18
1486	941	3.8×10^{-2}			

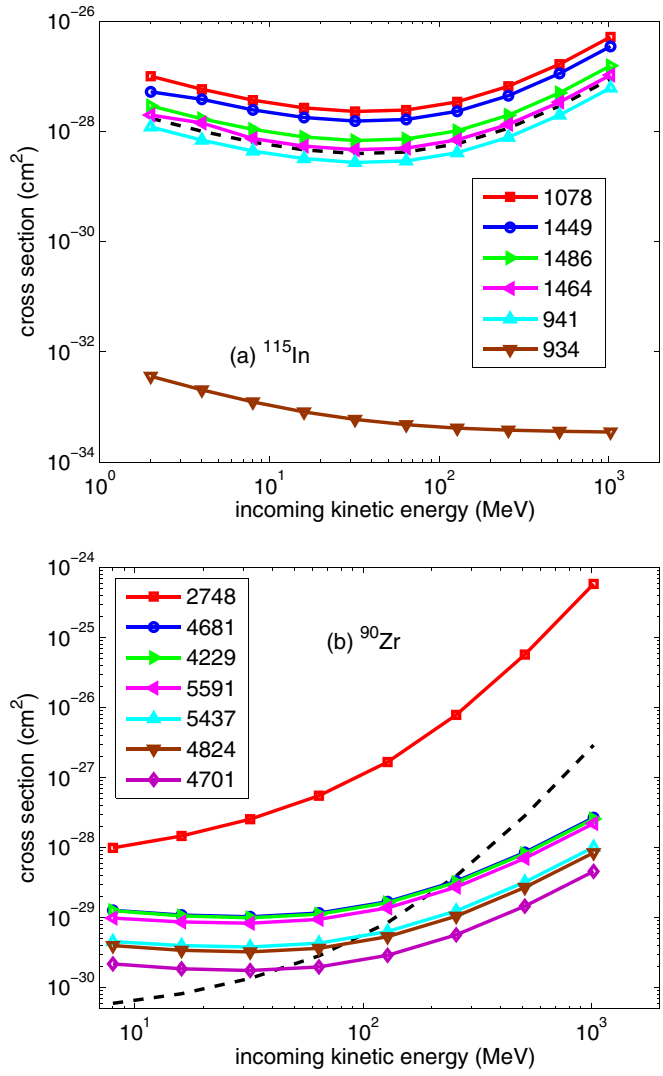

FIG. 2. Cross sections for nuclear excitation of (a) ^{115}In and (b) ^{90}Zr by muon scattering, showing transitions to various nuclear states labeled by their excitation energies (in keV). The dashed black curve in each panel indicates the effective excitation cross section to the 336-keV isomeric state of ^{115}In and the 2319-keV isomeric state of ^{90}Zr, respectively.

934-keV state of ^{115}In and the 2748-keV state of ^{90}Zr. In addition, the contribution of higher-order transition types is often significant, especially at high energies. For example, the $E3$-type cross section for ^{90}Zr to the 2748-keV state increases with incoming kinetic energy. While the $E2$-type cross sections also increase with incident energy above 100 MeV, their rates remain notably lower. In fact, under extreme relativistic conditions, the cross section follows the relation $\sigma_{if} \propto k_i^{2\lambda-2}$ according to Eq. (27), which is based on the Dirac plane-wave Born approximation (PWBA). This relationship is also observed in high-energy electron scattering, where calculation results are essentially unaffected by the approximation [31,32].

In this work, we include only the nuclear excited states listed in Tables I and II. While there are additional excited states at higher energies, we do not include them in our calculations due to the lack of data for the reduced transition probabilities B and the branching ratios b. Consequently, the effective cross sections presented for the isomeric states should be regarded as lower limits, with the true values likely being higher.

B. Cross sections for μ^-, μ^+, and electrons

In Fig. 3, we show the effective isomeric excitation cross section (to the 336-keV isomeric state of ^{115}In and the 2319-keV isomeric state of ^{90}Zr), as given in Eq. (23), for μ^-, μ^+, and electrons. We observe that the cross section for μ^- is higher than that for μ^+ and electrons. At low energies (on the order of 1–10 MeV), the difference between μ^- and electrons is roughly 4 orders of magnitude. At higher energies, approaching 10^3 MeV, the cross sections for all three particles converge to similar values.

These results are consistent with expectations. Muons are generally more likely to induce nuclear excitation due to their greater rest mass. However, this difference becomes negligible under extreme relativistic conditions. Specifically, μ^- shares many similarities with electron scattering [31,32], while μ^+ behaves similarly to other positively charged particles in Coulomb excitation [55,56]. Additionally, the nuclear excitation efficiency of μ^- is higher than that of μ^+, since the positive charge of μ^+makes it more difficult to approach the nucleus due to electrostatic repulsion.

C. Estimating the influence of muon penetration

As mentioned, Eq. (13) and the subsequent formulas are based on the approximation that the overlap between the muon wave function and the nuclear wave function is negligible, meaning that the muon's penetration into the nucleus is ignored. In this section, we evaluate the validity of this approximation and examine how much the nuclear excitation is affected by the muon's penetration into the nuclear volume.

If the muon wave function is described by the Dirac DWs, we are unaware of a rigorous general method to perform the integration as given in Eq. (12) without the non-overlap approximation. However, if the muon wave functions can be

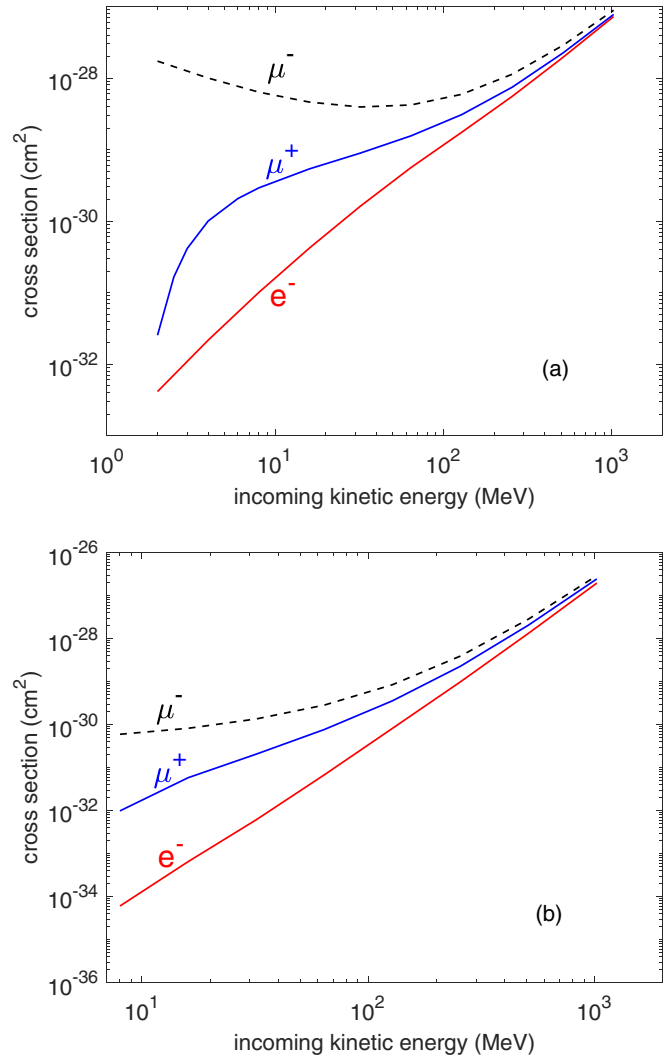

FIG. 3. Effective cross sections of isomer generation for (a) ^{115}In to the 336-keV state and (b) ^{90}Zr to the 2319-keV state. Black dashed, blue solid, and red solid lines represent the results of μ^-, μ^+, and electrons, respectively.

approximated as Dirac PWs,

$$\Phi_{\mathbf{k}} = u_{\mathbf{k}} \exp(i\mathbf{k}\cdot\mathbf{r}) = \frac{\exp(i\mathbf{k}\cdot\mathbf{r})}{4\pi}\sqrt{\frac{E+m_\mu c^2}{\pi E}}\begin{pmatrix}\chi_s\\ \frac{c\sigma\cdot\mathbf{k}}{E+m_\mu c^2}\chi_s\end{pmatrix}, \tag{25}$$

then the integration of Eq. (12) can be performed without the non-overlap approximation as [46]

$$\begin{aligned} F &= \int \frac{u_f^\dagger u_i \exp(i\mathbf{K}\cdot\mathbf{r}_\mu)\psi_f^*(\mathbf{r}_n)\psi_i(\mathbf{r}_n)}{|\mathbf{r}_n-\mathbf{r}_\mu|} d\mathbf{r}_\mu d\mathbf{r}_n \\ &= \frac{16\pi^2}{K^2}\sum_{lm} i^l u_f^\dagger u_i (-1)^m Y_{lm}(\theta_K,\varphi_K) \\ &\quad\times \int \psi_f^*(\mathbf{r}_n)\psi_i(\mathbf{r}_n) j_l(Kr_n) Y_{lm}^*(\theta_n,\varphi_n) d\mathbf{r}_n, \end{aligned} \tag{26}$$

where $\mathbf{K} = \mathbf{k}_i - \mathbf{k}_f$. The $E\lambda$-type cross section has the form

$$\sigma_{if} = \frac{8\pi^2(\lambda+1)B(E\lambda, i\to f)}{\lambda c^2 k_i^2[(2\lambda+1)!!]^2} \times \int_0^\pi K^{2\lambda}\left(V_T + \frac{\lambda}{\lambda+1}V_L\right)\sin\theta d\theta, \quad (27)$$

where θ denotes the angle between $\mathbf{k}_i$ and $\mathbf{k}_f$,

$$V_T = k_i k_f \frac{K^2\left(k_i^2+k_f^2-q^2\right) - 2(\mathbf{k}_i\cdot\mathbf{K})(\mathbf{k}_f\cdot\mathbf{K})}{K^2(K^2-q^2)^2},$$
$$V_L = k_i k_f \frac{2k_i^2+2k_f^2+4m_\mu^2c^2-q^2-K^2}{K^4}. \quad (28)$$

We can also accommodate muon penetration with the eikonal expansion [57]. Assuming the nuclear charge is evenly distributed in a sphere with radius R, we define an effective energy

$$\bar{E} = E + \frac{3Z}{2R} \quad (29)$$

and an effective momentum

$$\bar{k} = \sqrt{\frac{\bar{E}^2}{c^2} - m_\mu^2 c^2} \quad (30)$$

for the muon. The wave function in Eq. (25) becomes

$$\Phi_{\mathbf{k}} = \frac{\bar{k}}{k} u_{\mathbf{k}} \exp(i\bar{\mathbf{k}}\cdot\mathbf{r}), \quad (31)$$

which is known as the effective momentum approximation (EMA) [58]. Similarly, in the so-called modified effective momentum approximation (MEMA) [59–61], the wave function is written as

$$\Phi_{\mathbf{k}} = \sqrt{\frac{\bar{k}\bar{E}}{kE}} u_{\mathbf{k}} \exp(i\bar{\mathbf{k}}\cdot\mathbf{r}). \quad (32)$$

Similar to the above case using Dirac PWs, we can use these wave functions to derive the nuclear excitation cross sections without applying the non-overlap approximation. Specifically,

$$\sigma_{if} = \frac{8\pi^2\bar{k}_i^2\bar{k}_f^2(\lambda+1)B(E\lambda, i\to f)}{\lambda c^2 k_i^4 k_f^2[(2\lambda+1)!!]^2} \times \int_0^\pi \bar{K}^{2\lambda}\left(\bar{V}_T + \frac{\lambda}{\lambda+1}\bar{V}_L\right)\sin\theta d\theta \quad (33)$$

for EMA, and

$$\sigma_{if} = \frac{8\pi^2\bar{k}_i\bar{k}_f\bar{E}_i\bar{E}_f(\lambda+1)B(E\lambda, i\to f)}{\lambda c^2 k_i^3 k_f E_i E_f[(2\lambda+1)!!]^2} \times \int_0^\pi \bar{K}^{2\lambda}\left(\bar{V}_T + \frac{\lambda}{\lambda+1}\bar{V}_L\right)\sin\theta d\theta \quad (34)$$

for MEMA, where $\bar{\mathbf{K}} = \bar{\mathbf{k}}_i - \bar{\mathbf{k}}_f$ and

$$\bar{V}_T = k_i k_f \frac{\bar{K}^2\left(k_i^2+k_f^2-q^2\right) - 2(\mathbf{k}_i\cdot\bar{\mathbf{K}})(\mathbf{k}_f\cdot\bar{\mathbf{K}})}{\bar{K}^2(\bar{K}^2-q^2)^2},$$
$$\bar{V}_L = k_i k_f \frac{2k_i^2+2k_f^2+4m_\mu^2c^2-q^2-K^2}{\bar{K}^4}. \quad (35)$$

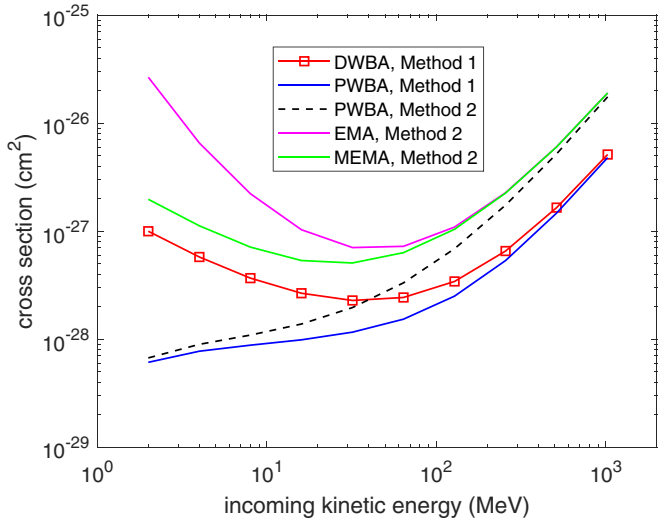

FIG. 4. Cross sections of nuclear excitation to the 1078-keV state of ^{115}In by muon scattering with two different classes of methods. Method 1 is introduced in Sec. II, where Eq. (18) is used in calculation and the penetration effect is absent. Method 2 uses Eqs. (27), (33), and (34), which take into account the muon penetration starting from different forms of wave functions.

Figure 4 compares the nuclear excitation cross sections to the 1078-keV state of ^{115}In using two different classes of methods. Method 1 is based on the non-overlap approximation whereas method 2 is not. The nuclear radius is taken to be 4.6 fm [62]. The red curve with square symbols [also shown in Fig. 2(a)] represents the DWBA method with the non-overlap approximation (DWBA, method 1). The solid blue curve corresponds to the PWBA method with the non-overlap approximation, obtained by setting $V(r) = 0$ in the DW method (PWBA, method 1). It is evident that these two curves agree at high energies, but the PW method underestimates the cross section by approximately an order of magnitude at low energies.

The other three curves are obtained without using the non-overlap approximation (i.e., Method 2), and muon penetration is taken into account as explained earlier. These three curves are obtained with Dirac PWs, the EMA, and the MEMA wave functions, respectively. We see that these three curves converge at high energies to cross-section values that are two or three times higher than the converged values from method 1, indicating that the difference arises from the penetration effect. At low energies, the penetration effect is expected to be small, as can be seen from the comparison between the two PWBA curves. The three curves from method 2 show relatively large differences at low energies, presumably due to the diverse theoretical approximations. Similar to previous reports, MEMA tends to be closer to PWs and EMA tends to be higher, overestimating the cross section [59].

IV. CONCLUSION

In this paper, we present a relativistic theoretical framework for calculating nuclear excitation induced by muon

beams, applicable across a wide range of muon energies from 1 to 1000 MeV. To make the framework more relevant to potential experiments, we focus on experimentally accessible isotopes, ^{115}In and ^{90}Zr, and calculate the effective cross sections for excitation to long-lifetime isomeric states, which are suitable for postexcitation detection. We also compare the excitation cross sections for μ^-, μ^+, and electrons. Additionally, we assess the impact of muon penetration into the nucleus on the nuclear excitation cross section, finding that it remains within a factor of 2 to 3 below 1 GeV.

ACKNOWLEDGMENTS

We acknowledge invaluable discussions with Professor Feng Zhang and Professor Wei Qi from the Laser Fusion Research Center of China Academy of Engineering Physics. This work was supported by NSFC Grants No. 12474484, No. U2330401, and No. 12088101.

DATA AVAILABILITY

The data that support the findings of this article are openly available [63].

[1] A. Antognini *et al.*, Proton structure from the measurement of 2S-2P transition frequencies of muonic hydrogen, Science **339**, 417 (2013).
[2] J. J. Krauth *et al.*, Measuring the α-particle charge radius with muonic helium-4 ions, Nature (London) **589**, 527 (2021).
[3] P. Strasser *et al.*, Improved measurements of muonic helium ground-state hyperfine structure at a near-zero magnetic field, Phys. Rev. Lett. **131**, 253003 (2023).
[4] R. L. Garwin, L. M. Lederman, and M. Weinrich, Observations of the failure of conservation of parity and charge conjugation in meson decays: the magnetic moment of the free muon, Phys. Rev. **105**, 1415 (1957).
[5] R. P. Singh, A. D. Hillier, B. Mazidian, J. Quintanilla, J. F. Annett, D. M. Paul, G. Balakrishnan, and M. R. Lees, Detection of time-reversal symmetry breaking in the noncentrosymmetric superconductor Re_6Zr using muon-spin spectroscopy, Phys. Rev. Lett. **112**, 107002 (2014).
[6] A. D. Hillier *et al.*, Muon spin spectroscopy, Nat. Rev. Methods Primers **2**, 4 (2022).
[7] K. N. Borozdin *et al.*, Radiographic imaging with cosmic-ray muons, Nature (London) **422**, 277 (2003).
[8] K. Morishima *et al.*, Discovery of a big void in Khufu's pyramid by observation of cosmic-ray muons, Nature (London) **552**, 386 (2017).
[9] S. Procureur *et al.*, Precise characterization of a corridor-shaped structure in Khufu's pyramid by observation of cosmic-ray muons, Nat. Commun. **14**, 1144 (2023).
[10] L. W. Alvarez *et al.*, Catalysis of nuclear reactions by μ mesons, Phys. Rev. **105**, 1127 (1957).
[11] T. Yamashita, Y. Kino, K. Okutsu, S. Okada, and M. Sato, Roles of resonant muonic molecule in new kinetics model and muon catalyzed fusion in compressed gas, Sci. Rep. **12**, 6393 (2022).
[12] A. Carne, S. F. J. Cox, G. H. Eaton, and C. A. Scott, The ISIS pulsed muon facility: Past, present and future, Hyperfine Interact. **65**, 1175 (1991).
[13] G. M. Marshall, Muon beams and facilities at TRIUMF, Z. Phys. C **56**, S226 (1992).
[14] A. Rafeal *et al.*, The μSR facilities at PSI, Hyperfine Interact. **87**, 1105 (1994).
[15] Y. Miyake *et al.*, J-PARC muon source, MUSE, Nucl. Instrum. Methods Phys. Res., Sect. A **600**, 22 (2009).
[16] S. Cook *et al.*, Delivering the world's most intense muon beam, Phys. Rev. Accel. Beams **20**, 030101 (2017).
[17] X. Zhou *et al.*, Status of the high-intensity heavy-ion accelerator facility in China, AAPPS Bull. **32**, 35 (2022).
[18] F. Zhang *et al.*, Proof-of-principle demonstration of muon production with an ultrashort high-intensity laser, Nat. Phys. **21**, 1050 (2025).
[19] L. Calvin *et al.*, Experimental evidence of production of directional muons from a laser-wakefield accelerator, Plasma Phys. Control. Fusion **68**, 035015 (2026).
[20] S. Gargiulo, M. F. Gu, F. Carbone, and I. Madan, Nuclear excitation by free muon capture, Phys. Rev. Lett. **129**, 142501 (2022).
[21] E. V. Tkalya, Cross section of the Coulomb excitation of ^{229m}Th by low energy muons, Chin. Phys. C **45**, 094102 (2021).
[22] A. Pálffy, W. Scheid, and Z. Harman, Theory of nuclear excitation by electron capture for heavy ions, Phys. Rev. A **73**, 012715 (2006).
[23] A. Pálffy, J. Evers, and C. H. Keitel, Isomer triggering via nuclear excitation by electron capture, Phys. Rev. Lett. **99**, 172502 (2007).
[24] J. Gunst, Y. A. Litvinov, C. H. Keitel, and A. Pálffy, Dominant secondary nuclear photoexcitation with the x-ray free-electron laser, Phys. Rev. Lett. **112**, 082501 (2014).
[25] A. V. Volotka, A. Surzhykov, S. Trotsenko, G. Plunien, T. Stöhlker, and S. Fritzsche, Nuclear excitation by two-photon electron transition, Phys. Rev. Lett. **117**, 243001 (2016).
[26] Y. Wu, J. Gunst, C. H. Keitel, and A. Pálffy, Tailoring laser-generated plasmas for efficient nuclear excitation by electron capture, Phys. Rev. Lett. **120**, 052504 (2018).
[27] Y. Wu, C. H. Keitel, and A. Pálffy, ^{93m}Mo isomer depletion via beam-based nuclear excitation by electron capture, Phys. Rev. Lett. **122**, 212501 (2019).
[28] E. V. Tkalya, Excitation of ^{229m}Th at inelastic scattering of low energy electrons, Phys. Rev. Lett. **124**, 242501 (2020).
[29] J. Rzadkiewicz, M. Polasik, K. Slabkowska, Ł. Syrocki, J. J. Carroll, and C. J. Chiara, Novel approach to ^{93m}Mo isomer depletion: Nuclear excitation by electron capture in resonant transfer process, Phys. Rev. Lett. **127**, 042501 (2021).
[30] S. Gargiulo, I. Madan, and F. Carbone, Nuclear excitation by electron capture in excited ions, Phys. Rev. Lett. **128**, 212502 (2022).
[31] H. Zhang, W. Wang, and X. Wang, Nuclear excitation cross section of ^{229}Th via inelastic electron scattering, Phys. Rev. C **106**, 044604 (2022).
[32] B. Liu and X. Wang, Isomeric excitation of ^{235}U by inelastic scattering of low-energy electrons, Phys. Rev. C **106**, 064604 (2022).

[33] J. Qi, H. Zhang, and X. Wang, Isomeric excitation of ^{229}Th in laser-heated clusters, Phys. Rev. Lett. **130**, 112501 (2023).

[34] H. Zhang and X. Wang, Theory of isomeric excitation of ^{229}Th via electronic processes, Front. Phys. **11**, 1166566 (2023).

[35] J. Qi, B. Liu, and X. Wang, Laser-based approach to verify nuclear excitation by electron capture, Phys. Rev. C **110**, L051601 (2024).

[36] J. Zhao, A. Pálffy, C. H. Keitel, and Y. Wu, Efficient production of ^{229m}Th via nuclear excitation by electron capture, Phys. Rev. C **110**, 014330 (2024).

[37] J. Feng *et al.*, Laser-based approach to measure small nuclear cross sections in plasma, Proc. Natl. Acad. Sci. USA **121**, e2413221121 (2024).

[38] W. C. Barber, F. Berthold, G. Fricke, and F. E. Gudden, Nuclear excitation by scattering of 40-Mev electrons, Phys. Rev. **120**, 2081 (1960).

[39] R. D. Edge and G. A. Peterson, Nuclear excitation by 180° electron scattering, Phys. Rev. **128**, 2750 (1962).

[40] C. J. Chiara *et al.*, Isomer depletion as experimental evidence of nuclear excitation by electron capture, Nature (London) **554**, 216 (2018).

[41] S. Guo, Y. Fang, X. Zhou, and C. M. Petrache, Possible overestimation of isomer depletion due to contamination, Nature (London) **594**, E1 (2021).

[42] S. Guo *et al.*, Probing ^{93m}Mo isomer depletion with an isomer beam, Phys. Rev. Lett. **128**, 242502 (2022).

[43] T. A. Griffy, D. S. Onley, J. T. Reynolds, and L. C. Biedenharn, Partial-wave analysis of the inelastic scattering of electrons by nuclei. I. Results for quadrupole excitations, Phys. Rev. **128**, 833 (1962).

[44] D. S. Onley, T. A. Griffy, and J. T. Reynolds, Partial-wave analysis of the inelastic scattering of electrons by nuclei. II. Application to the liquid drop model, Phys. Rev. **129**, 1689 (1963).

[45] D. S. Onley, T. A. Griffy, and J. T. Reynolds, Partial-wave analysis of the inelastic scattering of electrons by nuclei. III. Systematics of electric multipole excitation, Phys. Rev. **134**, B945 (1964).

[46] K. Alder, A. Bohr, T. Huus, B. Mottelson, and A. Winther, Study of nuclear structure by electromagnetic excitation with accelerated ions, Rev. Mod. Phys. **28**, 432 (1956).

[47] V. B. Berestetskii, E. M. Lifshitz, and L. P. Pitaevskii, *Quantum Electrodynamics* (Butterworth-Heinemann, Oxford, 1982), Vol. 4.

[48] F. Salvat and J. M. Fernández-Varea, RADIAL: A Fortran subroutine package for the solution of the RADIAL Schrödinger and Dirac wave equations, Comput. Phys. Commun. **240**, 165 (2019).

[49] C. A. Heras and S. M. Abecasis, Structure of $1f_{7/2}$ and $1g_{9/2}$ nuclei, Phys. Rev. C **12**, 1659 (1975).

[50] A. E. Stuchbery, N. Benczer-Koller, G. Kumbartzki, and T. J. Mertzimekis, Gyromagnetic ratios and octupole collectivity in the structure of the $^{90-96}$Zr isotopes, Phys. Rev. C **69**, 044302 (2004).

[51] Y. Hao *et al.*, Reinvestigation of the level structures of the even-even nuclei ^{90}Zr and ^{92}Zr, Phys. Rev. C **111**, 034312 (2025).

[52] D. C. Radford *et al.*, Coulomb excitation of radioactive ^{132,134,136}Te beams and the low $B(E2)$ of ^{136}Te, Phys. Rev. Lett. **88**, 222501 (2002).

[53] M. Abramowitz, I. A. Stegun, and R. H. Romer, *Handbook of Mathematical Functions with Formulas, Graphs, and Mathematical Tables* (National Bureau of Standards, Washington, D.C., 1964).

[54] Nuclear Structure and Decay Databases (2025), https://www.nndc.bnl.gov/.

[55] T. Li, H. Zhang, and X. Wang, Theory of Coulomb excitation of the ^{229}Th nucleus by protons, Phys. Rev. C **108**, L041602 (2023).

[56] Z. Li, T. Li, and X. Wang, Semiclassical approach for nuclear Coulomb excitation, Phys. Rev. C **110**, 024605 (2024).

[57] D. R. Yennie, F. L. Boos, Jr., and D. G. Ravenhall, Analytic distorted-wave approximation for high-energy electron scattering calculations, Phys. Rev. **137**, B882 (1965).

[58] M. Traini, S. Turck-Chièze, and A. Zghiche, Deep inelastic electron scattering in the distorted-wave Born approximation: An analytic approach, Phys. Rev. C **38**, 2799 (1988).

[59] J. Engel, Approximate treatment of lepton distortion in charged-current neutrino scattering from nuclei, Phys. Rev. C **57**, 2004 (1998).

[60] J. A. Tjon and S. J. Wallace, Coulomb corrections in quasielastic scattering based on the eikonal expansion for electron wave functions, Phys. Rev. C **74**, 064602 (2006).

[61] S. J. Wallace and J. A. Tjon, Coulomb corrections in quasi-elastic scattering: Tests of the effective-momentum approximation, Phys. Rev. C **78**, 044604 (2008).

[62] I. Angeli and K. P. Marinovab, Table of experimental nuclear ground state charge radii: An update, At. Data Nucl. Data Tables **99**, 69 (2013).

[63] J. Zhou, Figshare (2026), 10.6084/m9.figshare.30731324.v2.